



This is a repository copy of *Defining the role of 'zero wear volume' in percussive impact*.

White Rose Research Online URL for this paper:
<https://eprints.whiterose.ac.uk/167630/>

Version: Accepted Version

Article:

Zalzal, M., Lewis, R. orcid.org/0000-0002-4300-0540 and Slatter, T. orcid.org/0000-0002-0485-4615 (2021) Defining the role of 'zero wear volume' in percussive impact. *Wear*, 464-465. 203535. ISSN 0043-1648

<https://doi.org/10.1016/j.wear.2020.203535>

Article available under the terms of the CC-BY-NC-ND licence
(<https://creativecommons.org/licenses/by-nc-nd/4.0/>).

Reuse

This article is distributed under the terms of the Creative Commons Attribution-NonCommercial-NoDerivs (CC BY-NC-ND) licence. This licence only allows you to download this work and share it with others as long as you credit the authors, but you can't change the article in any way or use it commercially. More information and the full terms of the licence here: <https://creativecommons.org/licenses/>

Takedown

If you consider content in White Rose Research Online to be in breach of UK law, please notify us by emailing eprints@whiterose.ac.uk including the URL of the record and the reason for the withdrawal request.



eprints@whiterose.ac.uk
<https://eprints.whiterose.ac.uk/>

Defining The Role of “Zero Wear Volume” in Percussive Impact

Zalzalalah, M., Lewis, R., Slatter, T.*

Department of Mechanical Engineering, The University of Sheffield, Mappin Street, Sheffield, U.K. S1 3JD

* Corresponding author - tom.slatter@sheffield.ac.uk

Abstract: This work defines the previously undetermined contribution of the ‘zero wear’ volume, that is geometry change due to material compression that occurs before other mechanisms that cause change through actual material loss are initiated during repetitive impact. Five metal alloys widely used in engineering applications, each with a different bulk hardness, were the subjects of the experiments. Using a reciprocating hammer type impact wear test apparatus, flat coupon type specimens were subjected to repetitive impact from a chrome steel ball acting normal to the surface. 36,000 impacts were applied at a nominal rate of 10 impacts per second, each with an impact energy of 0.23J and an impact force of 3.5kN. The impact wear crater on selected worn specimens was examined using a 3D non-contact profilometer. Scanning electron microscopy techniques were used to further examine the damage on the specimens. The main damage mechanism was plastic deformation and surface fatigue due to spalling. Microcracks and adhered wear debris were noted on the specimens, but with no evidence of delamination, while subsurface examination showed no possible microcracks under the impacted surface and only surface pitting could be observed from subsurface examination. Analysis of the wear scars suggests that zero wear volume is the main contributor to the total volume ‘loss’ for all materials, and, for specific materials, plastic flow volume and bulk hardness could be a significant parameter in characterising zero-wear volume and crater depth.

Keywords: Percussive Impact Wear; Zero Wear Volume; Plastic flow; Surface Cracking; Spalling

1. Introduction

Wear and failure prediction are the most challenging tasks in the design and application of materials, and without sufficient knowledge of how the material fails it is difficult to improve its performance.

Impact wear, defined as wear of a surface that is due to percussion, which is a repetitive exposure to contact by another body [1], and also variously referred to as hammering wear or percussive wear is one of the least studied types of wear. Although it occurs in many engineering and industrial components, it has not been investigated as extensively as other wear mechanisms (e.g. abrasion, adhesion). Consequently, data on impact wear and its causes is quite scarce.

The overall volume loss due to wear for materials under repetitive impact can be measured directly either by mass scale (mass change) or by 3D non-contact profilometer (volume change). The former can determine very accurately the mass loss of materials, which can be converted to volume loss, it cannot indicate the components of the wear scar geometry, which include depth and width or radius. Neither can it predict the plastic flow volume of the ridges often present on the outer circumference of the wear scar. The latter can overcome those limitations but conversion of measurement data to the equivalent mass loss assumes uniform distribution of density. Extremes of surface geometry and reflectivity properties can also cause difficulties.

The only previous fundamental work of significance in this area is that of Engel which was conducted in the late 1970s. These studies initially defined, in terms of number of cycles, two stages that all materials undergo

throughout repetitive impacts. The first stage is an induction period, where no material is lost, and the end of this stage is defined as the zero wear limit (N_0), as shown in Figure 1. The second stage is the measurable wear region [2].

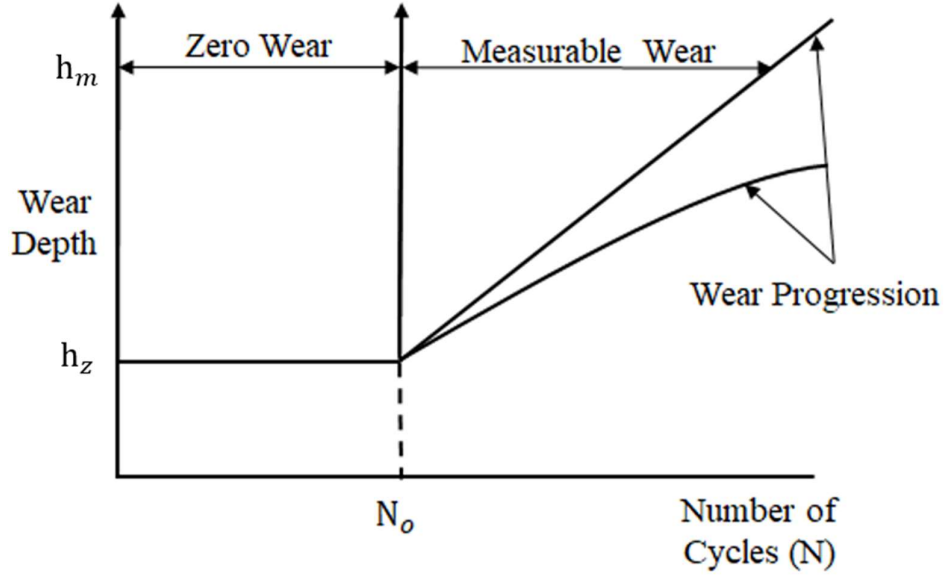


Figure 1 - Zero and measurable impact wear [2].

Engel then developed a model for steel specimens subjected to repetitive compound impacts in the elastic region to calculate the number of cycles at the zero wear limit [2-5].

Equation 1 was derived to evaluate the zero-wear limit for steel specimens subjected to repetitive compound impacts in the elastic region. It considers wear damage resulting from the surface shear stress, τ_2 , and the maximum subsurface shear stress, τ_1 , during each impact.

$$N_0 = \frac{1}{1+\beta} \left(\frac{\gamma \sigma_y}{P_0} \right)^9 2000 \quad (1)$$

where N_0 is the number of cycles at which the zero limit is reached; σ_y is the tensile yield stress; P_0 is the peak Hertzian contact pressure and γ is a material wear factor (approximately 1.1 for carbon and tool steel specimens) [4]. Equation 2 defines β as the ratio of subsurface damage D_1 (Equation 3) and the surface damage D_2 (Equation 4):

$$\beta = \frac{D_2}{D_1} \quad (2)$$

$$D_1 = \int_0^{t^*} \tau_1^9(t) dt \quad (3)$$

$$D_2 = \int_0^{\bar{t}} \tau_2^9(t) dt \quad (4)$$

and t^* is the contact time and \bar{t} is the slipping time.

This zero-wear model can only be applied when the contact is elastic in nature, but cannot predict the maximum scar depth at the zero wear limit. Additionally, the model can only predict the number of zero wear cycles,

whereas in reality materials under plastic deformation will go through a number of cycles before they start to wear.

Therefore, the model has three main limitations, first it can only be used to predict the number of cycles at which the zero limit is reached when the contact is elastic in nature and therefore the maximum contact pressure should be below or equal to the yield stress of material. In reality materials in the plastic region will go through a further number of cycles before they start to wear. Previous experimental work by the authors on stainless steel (AISI 304) at 10Hz using an impact hammering wear rig proved that, after very small number of cycles (20-30), an apparent deformed contact region forms in the plastic region without any mass loss. Furthermore, after significantly more cycles (16800) no mass loss was recorded, but a large scar was formed. Also, it cannot predict the maximum scar depth at the zero wear limit whether it is in the elastic or plastic region, and it can only predict the total number of zero wear cycles.

The work presented here employed both mass scales and non-contact profilometry in determining the zero-wear volume, which has not been defined previously as a part of overall volume loss for wear of materials under repetitive impacts.

It should be noted at this point that throughout this paper the following terms are used (and illustrated in Figure 2):

- *Wear Volume* – volume of material removed from the test specimen. Usually observed as wear debris that has detached from the specimen surface. A common measurement of ‘wear’ by mass loss measurements.
- *Plastic Flow Volume* – material removed plastically and ‘lost’ out of the contact zone, and therefore now not part of the material directly supporting a load, as a result of impact. Usually observed as newly formed ridges of material around the circumference of any resulting wear scar and not detected by mass loss methods.
- *Zero Wear Volume* – the volume previously occupied by material that appears to have been deformed by impact, causing its surface to be at a different point in space, but remains in the contact zone.
- *Total Volume Loss* – the sum of these volumes representing the space in which the wear volume, plastic flow volume, and zero wear volume previously resided.

The data for mass lost due to the wear was obtained from mass scale measurements of the specimens and was then used to calculate ‘wear volume’ by converting those masses to volumes with reference to the standard densities of the materials.

The total volume loss was calculated directly from the non-contact profilometer dataset. Assuming that the total volume loss can be considered as described by Equation 5, the zero wear volume can then be calculated from Equation 6 and as illustrated in Figure 2.

$$\text{Total Volume Loss } (V_t) = \text{Plastic Flow Volume } (V_{pf}) + \text{Wear Volume } (V_w) + \text{Zero Wear Volume } (V_{zw}) \quad (5)$$

$$V_{zw} = V_t - V_{pf} - V_w \quad (6)$$

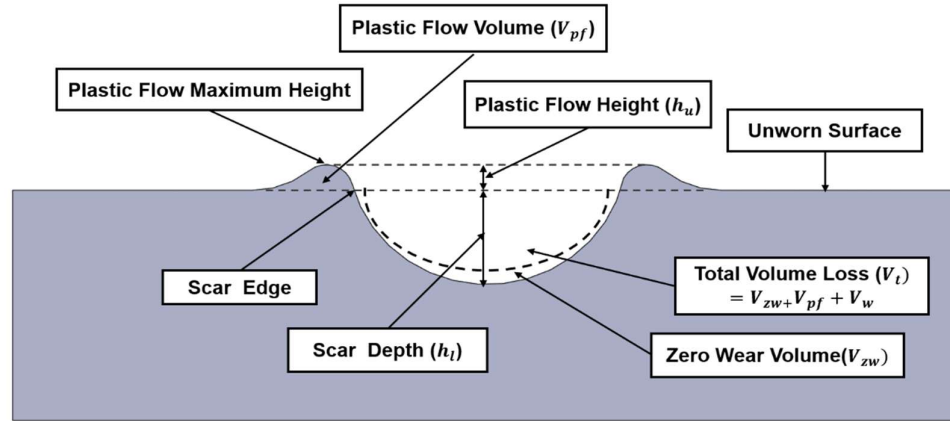


Figure 2 - Schematic illustrating the total volume loss during impact.

2. Materials and Methods

2.1. Test Apparatus

In order to ensure that the impact would repeatedly occur in the same contact region, thus reflecting the actual contact mechanism of components, and to enable a detailed study of that region under different impact parameters, a modified version of the reciprocating hammer type impact wear apparatus initially designed and then used previously by the authors [6-8] was used for this work.

A pancake type load cell was used to measure the impact force during each contact. It was placed directly below the specimen and the selected load cell can measure the load within the range 5N to 5000N (the expected range in this work). The response of the cell is acquired by digital data acquisition system with sampling frequency of 4.8kHz, selected so as to ensure that the true impact force is measured during the impact and can capture the rebounds efficiently.

A schematic is shown in Figure 3, illustrating the striker arm, made from silver steel to improve the stiffness, the cam and follower with helical stainless-steel compression spring. The majority of the rig was made from mild steel, except for the pivotal block and striker block which were made from aluminium alloy to reduce flexural bending of the arm throughout and to reduce the mass at the end of the arm.

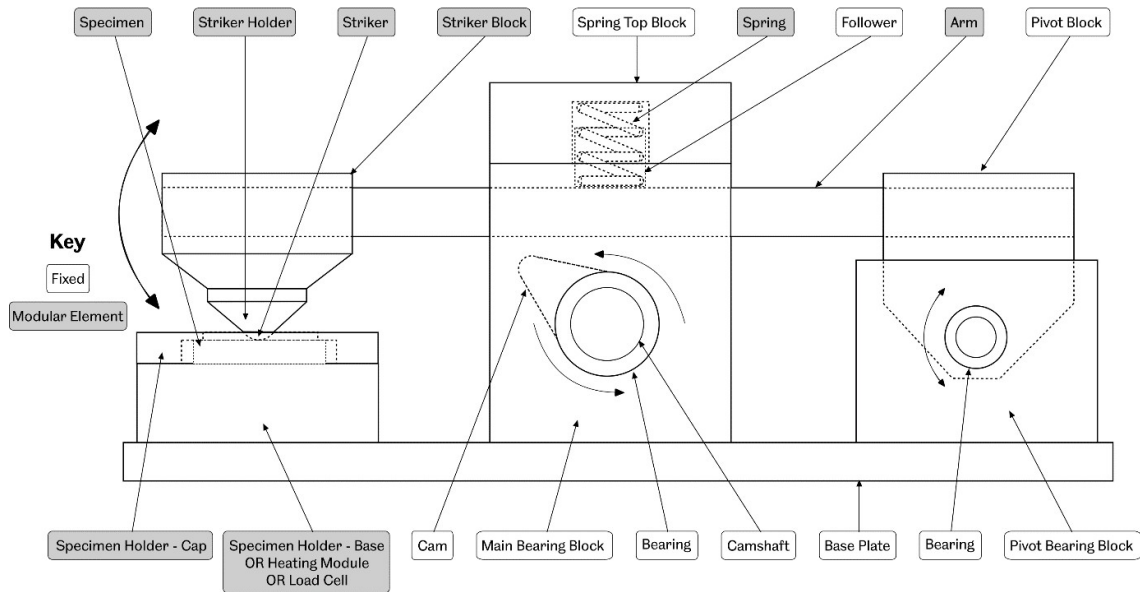


Figure 3 - Schematic diagram of impact wear rig [9].

The rig is driven by a 1.1 kW electrical motor and the speed of the motor is regulated by a variable frequency controller (inverter). The striker holder at the end of the lever arm secures in place a 15mm diameter stainless AISI 52100 steel ball with a maximum surface roughness of $R_a=(0.125\mu\text{m})$ that impinges on the surface of the test specimen. The selection of this particular striker is arbitrary for the work conducted here, but it has been extensively used in the previous work performed on this apparatus where it was selected to be representative of the contact(s) being studied and shown to consistently reproduce the required levels of measurable wear needed for this study

2.2. Test Specimens

Five different metal alloys widely used in engineering and industrial applications were used in this work; an austenitic stainless steel (AISI 304); a ductile cast iron (EN-GJS-600-3); a medium carbon steel (EN8); an aluminium alloy (AISI₉Cu₃) and a phosphor bronze (PB102). All specimens were cut from as received long round bars to form discs all with the dimensions of 50mm diameter and 10mm thickness. The mechanical properties and chemical composition of these materials as provided by their respective manufacturers is shown in Table 1 and Table 2 respectively. Bulk hardness was measured for all materials using a Vickers hardness tester (20kgf).

Material	Elongation %	Yield strength σ_y (MPa)	Tensile strength σ_u (MPa)	Young's Modulus (GPa)	Bulk Hardness (H_v)
Austenitic stainless steel (AISI 304)	58	270	581	190	190
Medium carbon steel (EN8)	10	628	739	200	211
Aluminum alloy (AISI ₉ Cu ₃)	~ 1	165	330	70	124
Ductile cast iron (EN-GJS-600-3)	3	370	600	174	238
Phosphor Bronze (PB102)	12-14	380	460	121	127
Chrome steel (AISI 52100) (ball)		2000	2300	210	700-900

Table 1 - Mechanical properties of tested materials and striker ball

Material	% wt.													Bal.
	C	Sn	Si	Mn	Cr	Ni	Cu	Mo	Mg	Zn	S	P	N	
Specimens														
AISI 304	0.03	-	0.43	1.04	18	9.36	-	0.42	-	-	0.026	0.029	0.062	Fe
EN8	0.43	-	0.2	0.72	0.02	0.06	-	-	-	-	0.021	0.013	-	Fe
AISI9Cu3	-	-	10.7	0.022	-	-	2.4	-	0.022	1.1	-	-	-	Al
EN-GJS-600-3	3.25-3.7		2.4-3	0.1-0.3	-	-	-	-	-	-	0.02 max	0.015-0.08	-	Fe
PB102	-	4.5-5.5	-	-	-	-	-	-	-	0.3 max	-	0.03-0.4	-	Cu
AISI 52100 (striker ball)	0.95-1.1		0.15-0.3	0.25 Max	1.3-1.6						0.025 Max	0.03 Max		

Table 2 - Elemental composition of specimen materials and striker ball.

2.3. Test Procedure

All the specimens were impacted with a frequency of 10Hz and average impact velocity of 0.62m/s (measured by high speed camera (Phantom V210)) and impact energy of 0.23J (calculated using the effective mass of the overall system (1.19kg)). Using a high-speed camera, it was found that the maximum height for the striker before impact was 10mm and the time required for the first impact was approximately 0.017sec.

Within each test cycle giving a nominal single impact, the high speed camera was able to capture four rebounds per each cam rotation. Due to the close proximity to each other of the specimen and striker ball at the moment of the fourth rebound, data from a pancake type load cell was used to confirm the existence of that rebound. If the extra recorded rebounds are considered as extra energy added to the specimen during each test apparatus cycle, the total impact energy per nominal 'impact' is actually 0.31J.

All materials were impacted with 36,000 cycles and the tests were repeated four times. The striker ball was replaced after each test and the specimens were cleaned with isopropanol before and after.

Both mass scale and 3D non-contact profilometer (Alicona SL, 5x objective) were used to take measurements to derive zero wear volume. The non-contact profilometer was also used to obtain wear scar measurements (diameter, depth) in addition to the volume of plastic flow, and the formation of plastic flow on the scar edges was also examined by optical microscope. All wear scar measurements were repeated a further three times and the data averaged. No blinding was performed.

The samples were sectioned and then ground with silicon carbide abrasive papers in four stages and then polished using 6 μm , 3 μm , 1 μm , and finally 0.25 μm diamond suspensions. Optical and scanning electron microscopy (SEM) techniques were then used to examine the damage, and micro-hardness profiles were taken subsurface in the wear scars as an increase in hardness was expected due to work hardening.

3. Stress Analysis for Point Contact

The two main parameters controlling the impact wear on the material surface are impact energy and contact stresses caused by the impact force which are dynamic in nature and vary continuously with impact time and area, that in thus vary with the deformation of the surface of a specimen.

Using the load cell the average peak impact force for the stainless steel used here, under normal impact, was recorded to have a value of 3476N and the impact time 0.83ms, then the maximum contact pressure and

subsurface stresses (von Mises and Tresca) were calculated using Hertzian analysis (based in MATLAB) for a point contact to indicate the likely nature of the contact (elastic, elastic-plastic or fully plastic) [10, 11]. A summary of results is provided in Table 3 for all materials and Figure 4 provides stress distribution plots (surface and subsurface) in austenitic stainless steel, under the conditions described in Section 2, as an example.

Materials	σ_y MPa	σ_u MPa	p_o MPa	p_m MPa	p_m/σ_y	σ_z MPa	σ_r MPa	σ_θ MPa	τ_{max} MPa	V_m MPa	Depth of max subsurface stresses from contact surface (mm)
AISI 304	270	581	5215	3476	13	5215	4119	4119	1628	3257	0.27
EN8	628	739	5308	3538	5.6	5308	4193	4193	1658	3315	0.267
AISI9Cu3	165	330	3446	2297	14	3446	2722	2722	1076	2152	0.33
EN-GJS-600-3	370	600	5036	3357	9	5036	3979	3979	1573	3145	0.27
PB102	380	460	4444	2963	7.8	4444	3511	3511	1388	2776	0.29

Table 3 - Surface and subsurface stresses for different materials.

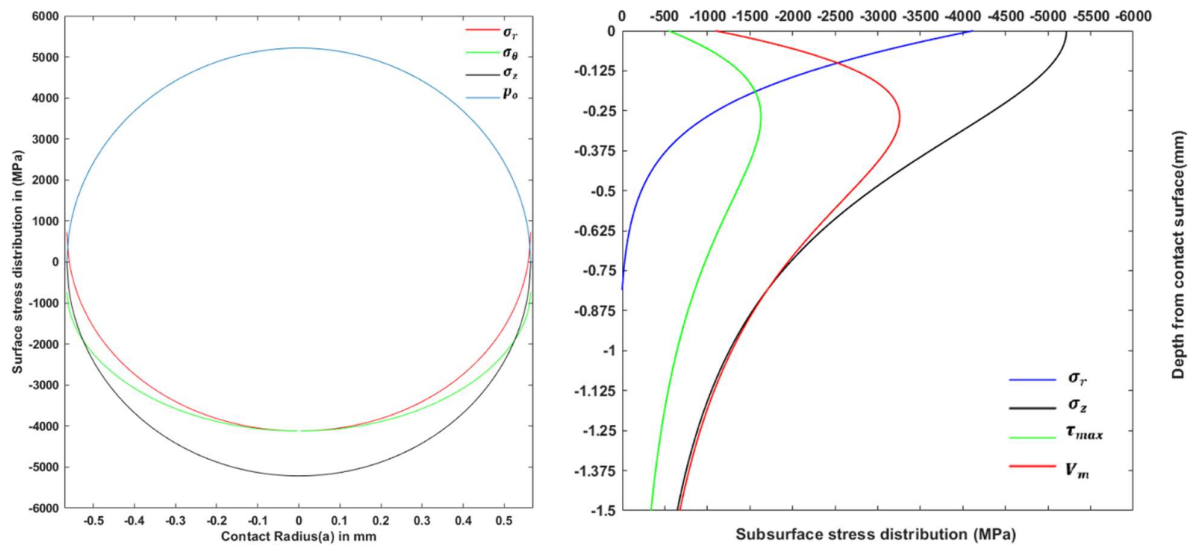


Figure 4 - Surface and subsurface stresses for austenitic stainless steel.

Materials under point contact are considered to be in the elastic region if the mean contact pressure p_m is less than $(1.1) \sigma_y$ [12] or p_o less than $1.6 \sigma_y$ [10, 13, 14]; at this ratio the material starts to be in elastic-plastic contact and the limit between the elastic-plastic region and fully plastic region can be defined as $1.1 < p_m/\sigma_y < 2.8$; when the ratio of p_m/σ_y exceeds 2.8, the material is considered to be in fully plastic [12]. Results revealed that the mean contact pressure exceeds the yield stress by (5.6-16.8) times (see Table 3); therefore, the nature of the contact used in this work could be considered as plastic throughout. That said, this is clearly an idealised analysis and further insight to the contact could be achieved by means of a finite element analysis which would facilitate the use of a more accurate representation of the plasticity in each of the materials used.

4. Results

4.1. Volume Loss

The results of the wear tests after 36,000 cycles were calculated by using Equations 5 and 6 using the following measurements;

- *Wear Volume* (V_w) (precision mass scale and then converted to volume loss through material density).
- *Plastic flow volume* (V_{pf}) (direct measurement by 3D non-contact profilometry)
- *Total Volume Loss* (V_t) (direct measurement by 3D non-contact profilometry)

In all cases, the sum of wear volume and plastic flow volume is significantly less than the directly measured total volume loss, and it is this difference that is defined as the zero wear volume defined earlier. This zero wear volume (V_{zw}) was calculated using Equation 6, and shown in Table 4. Figure 5 illustrates that the zero wear volume was the main contributor to the total volume loss (the total height of the bars) for all materials. For medium carbon steel and ductile cast iron plastic flow volume also contributed similarly (Equation 5).

Material	Elongation %	Mean Wear Volume (mm^3)	Mean Plastic Flow Volume (mm^3)	Mean Total Volume Loss (mm^3)	Mean Zero Wear Volume (mm^3)
AISI 304	58	0.0426	0.026	2.08	2.01
EN8	10	0.0505	0.753	1.527	0.72
AlSi9Cu3	1	0.15	0.0693	4.49	4.26
EN-GJS-600-3	3	0.0996	0.156	0.376	0.12
PB102	12	0.139	0.00482	4.134	3.99

Table 4 - Volume loss of different materials after 36,000 cycles under normal impact.

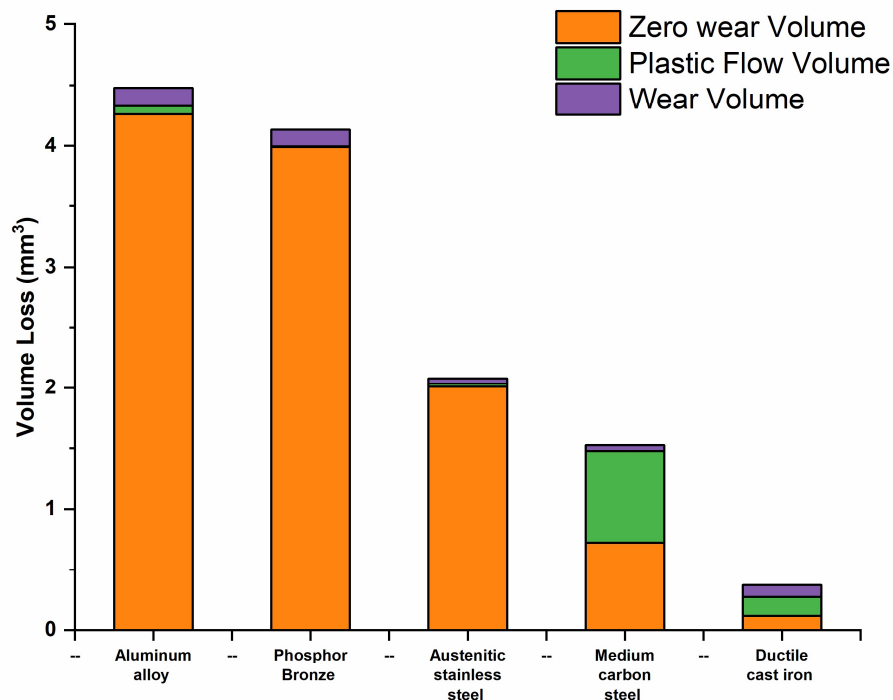


Figure 5 - Mean total volume loss, and of each component of the volume loss, for materials after 36,000 cycles.

It is surprising that the measured difference, and therefore the zero wear, is so large relative to the other measurements. The measured size of the plastic flow volume (the material that can be observed as ridges or extruded shoulders around the wear scar) cannot account all of the material that is 'missing' from the area of observable deformation, and indeed for stainless steel there is very little material like this to be observed (Figure 6). Equally, given that metal plasticity is generally assumed to be incompressible, it seems unlikely that this entirely due to the material being compressed under the impact, however, for the deformations shown in Figure 6, there was no mass loss measured and negligible deformation to the surface beyond the edges of the wear scar. Depending on the route and quality of manufacture there may be some subsurface imperfections that could account for some localised compression of the material.

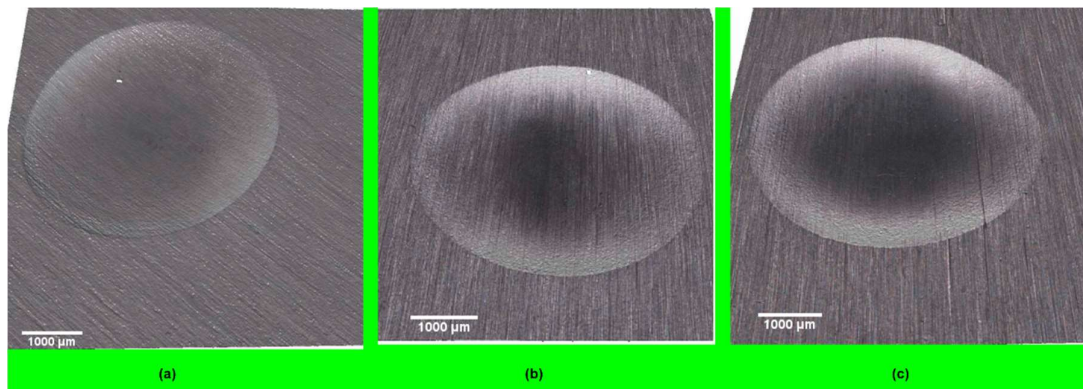


Figure 6 - Plastic deformation and apparent contact area of austenitic stainless steel under normal impact after (a) 1800 cycle; (b) 9,000 cycle and (c) 16,800 cycle

Figure 5 also illustrates that zero wear volume is almost equal to total volume loss for aluminium alloy, phosphor bronze and austenitic stainless steel, while for medium carbon steel and ductile cast iron the volume losses due to compression and plastic flow are approximately equal.

These results also suggest that materials with high ductility, such as austenitic stainless steel, may not necessarily have more plastic flow than other materials. This could be explained by the contribution of the zero wear volume, whereby a decrease in the total and zero wear volumes of both medium carbon steel and ductile cast iron led to a significant increase in plastic flow volume.

4.2. Mass Loss and Bulk Hardness

All materials showed a small amount of mass loss under repetitive impact for 36,000 cycles. Thus wear volume loss eventually represented the least mass loss for all materials due to the synergistic effect of zero wear volume and plastic flow volume, as illustrated in Figure 7.

The mean wear volume was calculated from mass loss based on the mass scale measurements and mean measured density of each material. The error bars represent the standard deviation of the data from four repetitions on specimens of each material type.

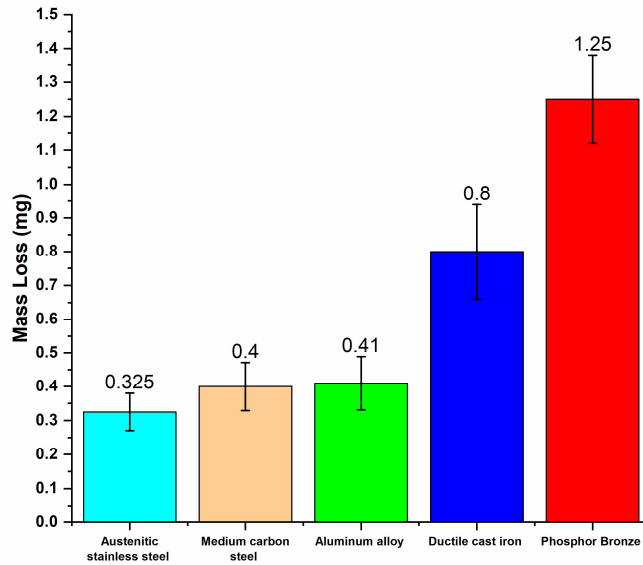


Figure 7 - Mean mass loss of different materials after 36,000 cycles.

Despite the fact that austenitic stainless steel is a relatively soft material, it showed the least mass loss among all tested materials which can be connected to its high ductility. Ductile cast iron with the highest bulk hardness ($238H_v$), showed more mass loss than both the medium carbon steel ($211H_v$) and the stainless steel ($190H_v$), as shown in Figure 8, which agrees with the work of Rabinowicz [15], the current results showed there is no direct correlation between the mass loss and bulk hardness, however further analysis of hardness at ultimate tensile strength for each material would provide more subtlety to this.

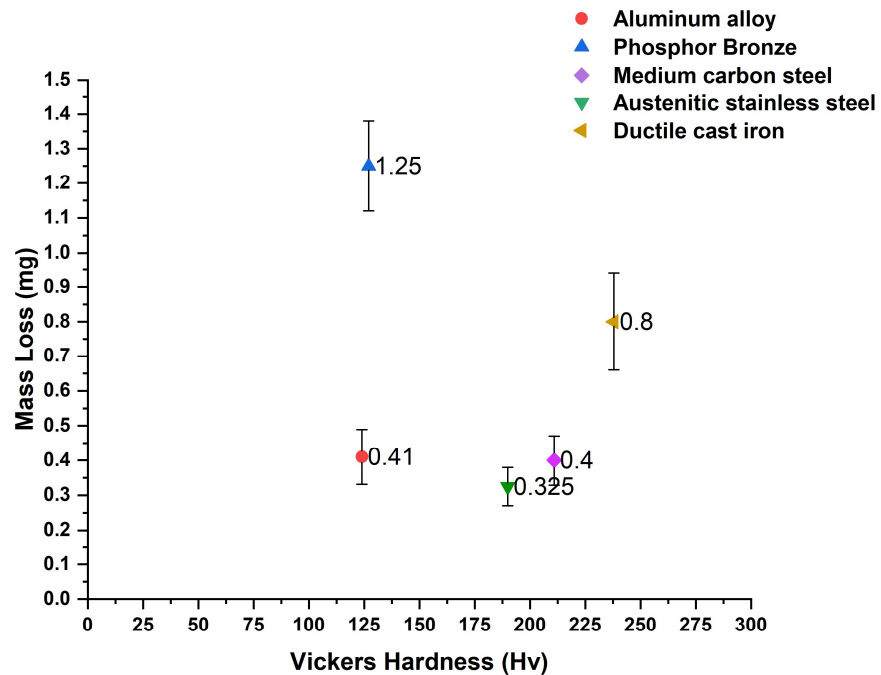


Figure 8 - Correlation between bulk hardness and mass loss for different materials after 36,000 cycles.

4.3. Zero Wear Volume and Total Volume Loss with Bulk Hardness

The results obtained suggest total volume loss and zero wear volume are all inversely proportional to hardness (see Figure 9 and Figure 10). The material of highest hardness, the ductile cast iron, gave the minimum indentation and volume loss, contrasting with results for both aluminium alloy and phosphor bronze.

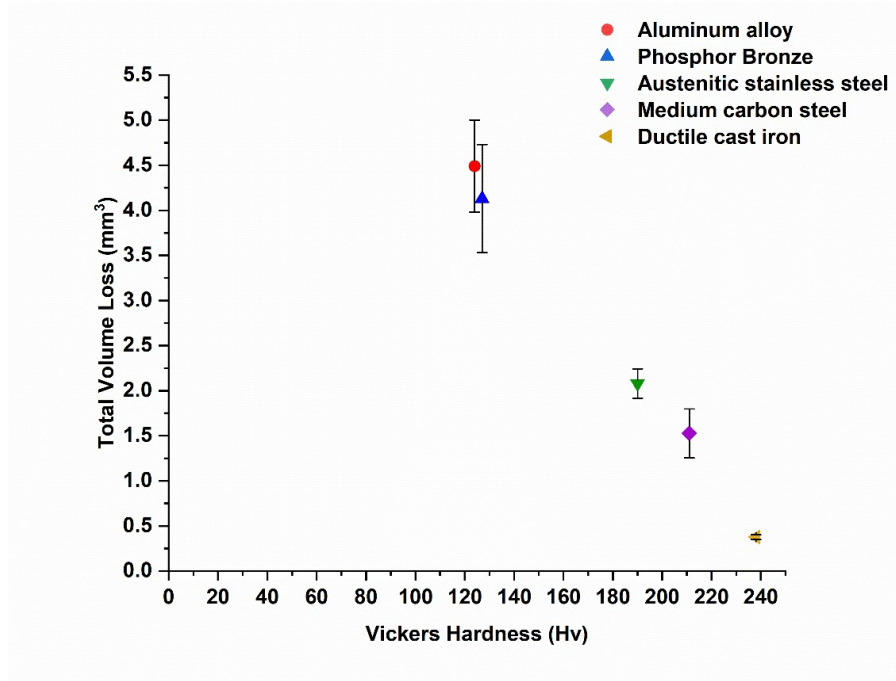


Figure 9 - Total volume loss of materials after 36000 cycles.

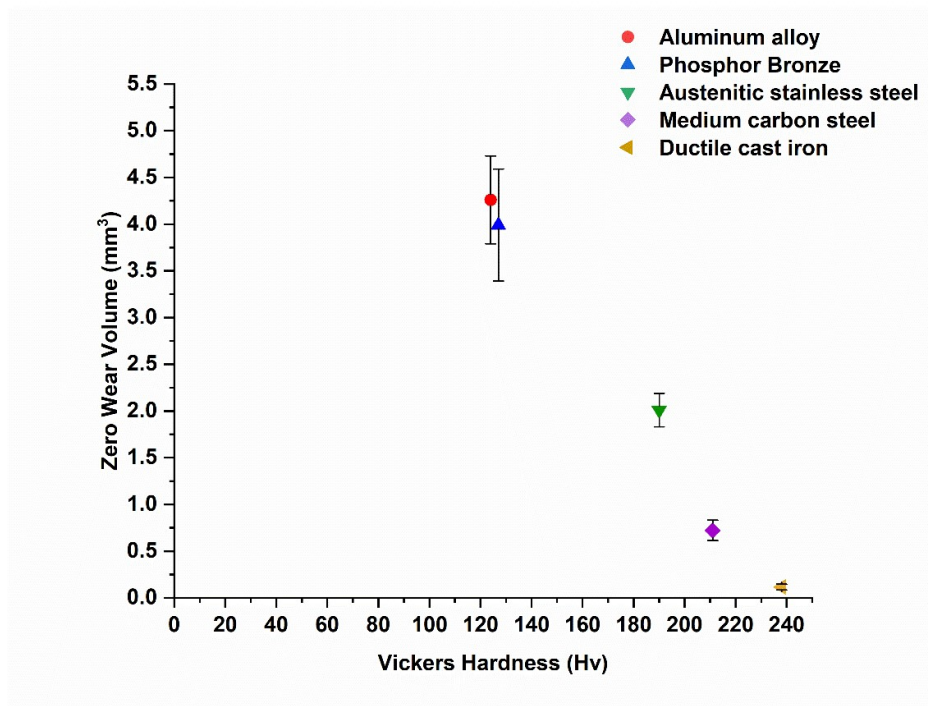


Figure 10 - Zero wear volume loss of materials after 36,000 cycles.

Figure 11 shows the scanned surface of the medium carbon steel sample after 36,000 cycles. The red coloured area in the centre of the figure represents the depth of the crater and both green and yellow represent the plastic flow above surface around the edge of the wear scar.

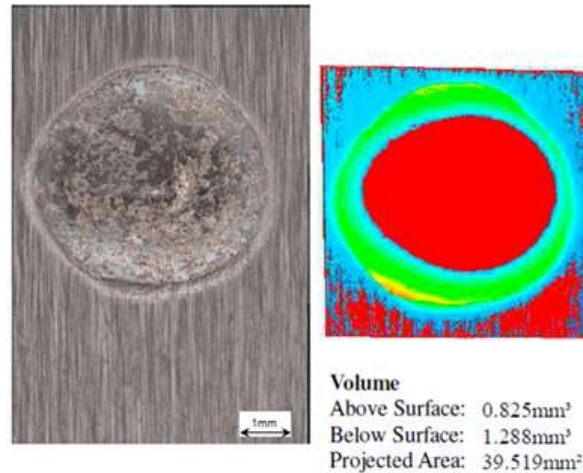


Figure 11 - Total volume as measured on a worn medium carbon steel (reference plane (blue), 'above surface' (green) = plastic flow volume and 'below surface' (red) = total volume loss).

These results agree to a great extent with previous results obtained by Wang et al. [16], where a 3D non-contact profilometer was also used to measure wear volume loss directly. They found that there was more volume loss in a soft aluminium alloy than an iron, but the iron lost more volume than tungsten. However, that study did not use a mass scale to compare between the two methods or identify the ratio of zero wear volume and total volume loss, therefore conflating wear volume and total volume loss to be equal.

4.4. Impact Wear Scar Measurements

4.4.1. Direct Measurement of Impact Wear Scar Diameter

The sizes of the impact wear scars were measured using the 3D non-contact profilometer. Every specimen was measured across three different directions across the diameter of the impact wear scar using the instrument's software analysis tools. The average for each specimen was recorded and then the averages of four repetitions were plotted as shown in Figure 12. This illustrates that the ductile cast iron, which has the highest hardness, has diameter approximately 40% less than that of aluminium alloy. This figure illustrates the role of hardness, providing approximately similar readings of impact wear scar diameter for aluminium alloy and phosphor bronze or medium carbon steel and austenitic stainless steel due to hardness similarity.

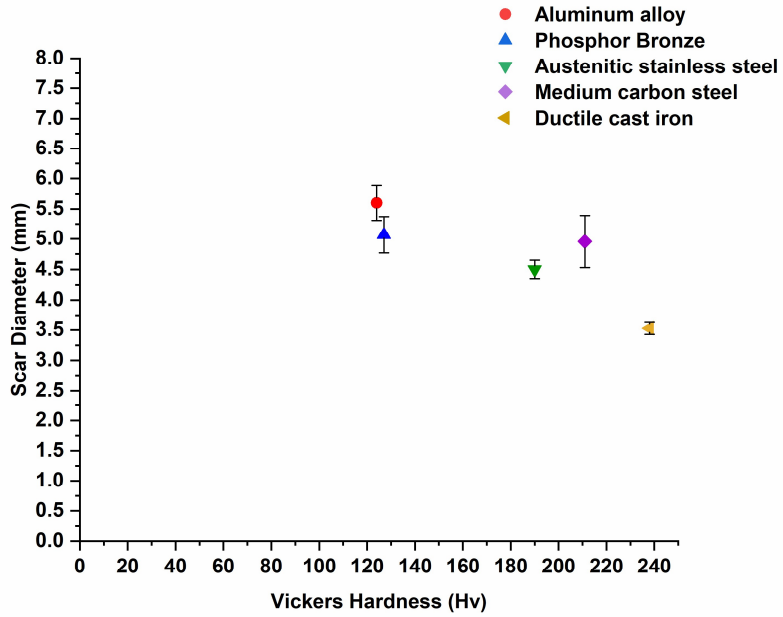


Figure 12 - Correlation between hardness and impact wear crater diameter after 36,000 cycles.

4.4.2. Direct Measurements of Impact Wear Scar Depth

To confirm the results of impact wear scar diameter and to measure the scar depth, the data from every diametric measurement was further analysed to produce geometric profiles of the scars. Measurements of the maximum and diameter of the impact scar for every material were taken and a typical profile for each material are shown in Figure 13.

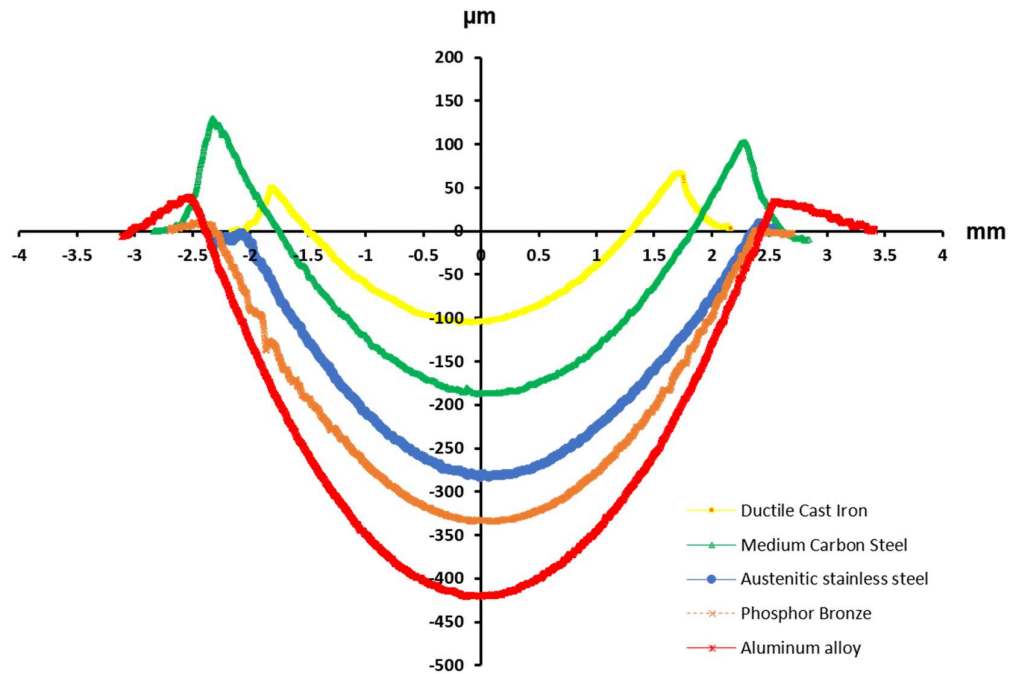


Figure 13 - Typical wear scar profile after 36,000 cycles for each material tested.

Figure 13 reveals, in general, the smooth surface profile of the materials' scars with some obvious rough surface on the near the edges of phosphor bronze, medium carbon steel and ductile cast iron have obvious plastic flow on the shoulders of the impact scar in addition to some plastic flow for aluminium alloy, while no obvious plastic flow is apparent for either austenitic stainless steel or phosphor bronze.

In terms of the test results recorded for each material, medium carbon steel produced the maximum plastic flow height (h_u) of 160 μm with maximum depth (h_l) of 263 μm and the plastic flow volume represents approximately 50% of the total volume loss; ductile cast iron produced a similar pattern with maximum (h_u) 71 μm and (h_l) of 117 μm , with plastic flow volume representing approximately 41% of total volume loss. Despite the plastic flow formation for the aluminium alloy, this was considered a small amount as the maximum plastic flow was only 80 μm , while the maximum depth was 426 μm .

The further analysis of the exported data confirmed the scar depths reported by the instrument's analysis software.

4.5. Impact Wear Scar Morphology

Despite the relatively low wear volume (i.e. material actually removed of the specimen) experienced by all materials tested, due to the dominance of zero wear volume and plastic flow volume in the total volume loss, damage to the surface of all the specimens was clear to the naked eye.

The impact scars were generally circular in shape for all materials although some exhibited significant ovality (particularly the stainless steel), which is likely due to the different mechanical properties leading to more plastic deformation [17]. All materials except austenitic stainless steel have low ductility of 12% or below while the stainless steel has high ductility (58%) which most likely explains this. The significant difference between the yield stress and the yield strength of this materials (310 MPa), the highest of the tested materials, also gives evidence as to why this occurs.

The typical wear scars for all materials can be seen in Figure 14. Figure 15 shows the wear damage mechanism in the centre region of the impact scar of all tested materials. Subsurface examination at the centre of the wear scars showed no signs of microcracks initiating below surface and then propagating up to the surface.

The main wear damage mechanism after 36,000 cycles was plastic deformation, either in the centre of the wear scar or on the impact shoulder as both Figure 15 and Figure 16 reveal. Plastic flow and surface fatigue, evidenced by spalling in the centre of the impact scar, were expected due to the maximum contact pressure in the middle of the contact region.

The results support the hypothesis that crack initiation at the surface and then propagation beneath the surface led to surface fatigue and eventual removal of material from the surface as wear debris due to spalling, with no obvious delamination or material transfer detected for any of the materials. Both medium carbon steel and ductile cast iron revealed a significant plastic flow on the ridges of wear scar.

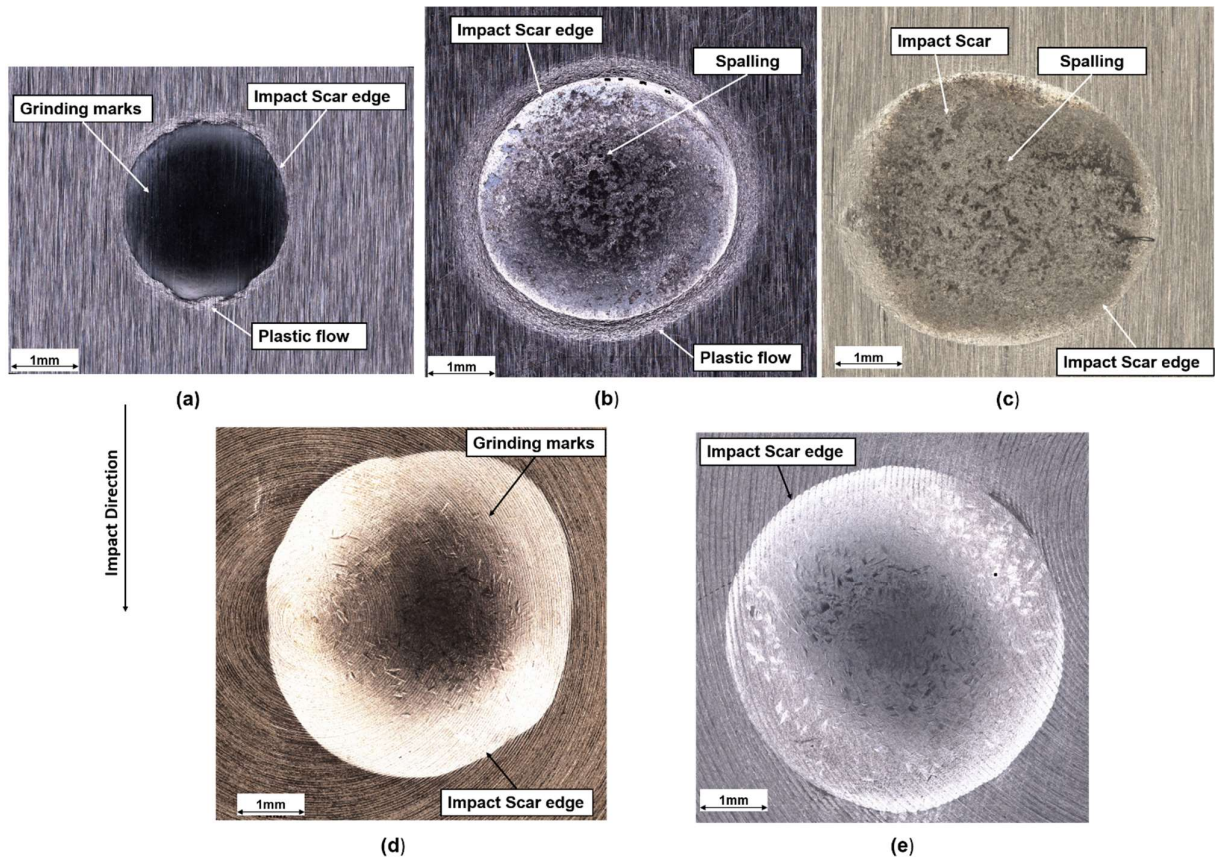


Figure 14 - Typical impact wear scar for tested materials after 36000 cycles for (a) ductile cast iron, (b) medium carbon steel, (c) austenitic stainless steel, (d) phosphor bronze and (e) aluminium alloy.

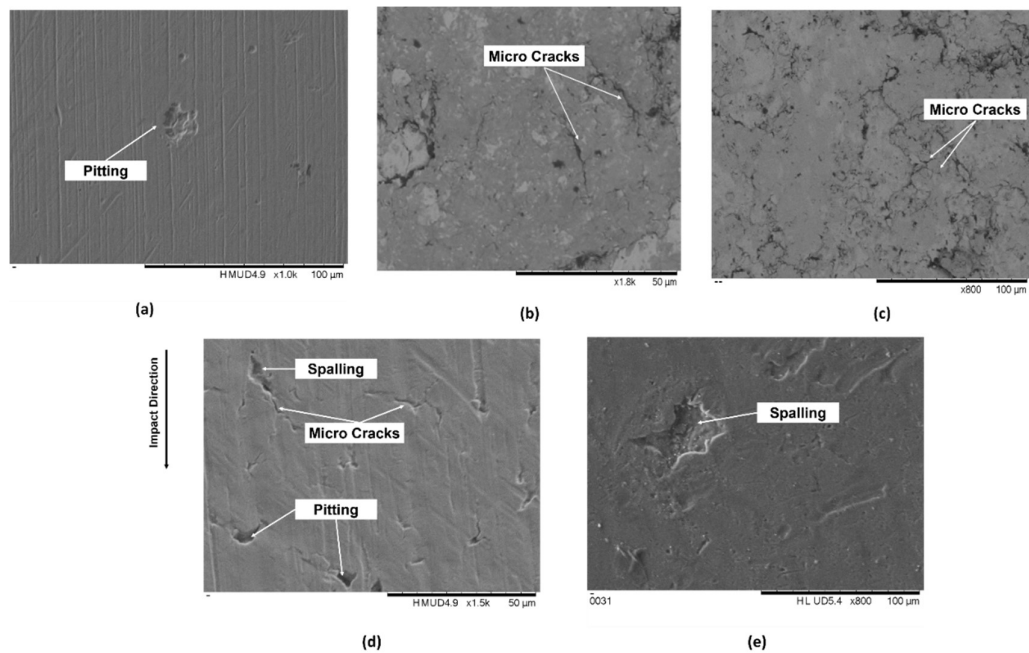


Figure 15 - Damage mechanism in the centre of the impact scar for tested materials after 36000 cycles for (a) ductile cast iron, (b) medium carbon steel, (c) austenitic stainless steel, (d) phosphor bronze and (e) aluminium alloy.

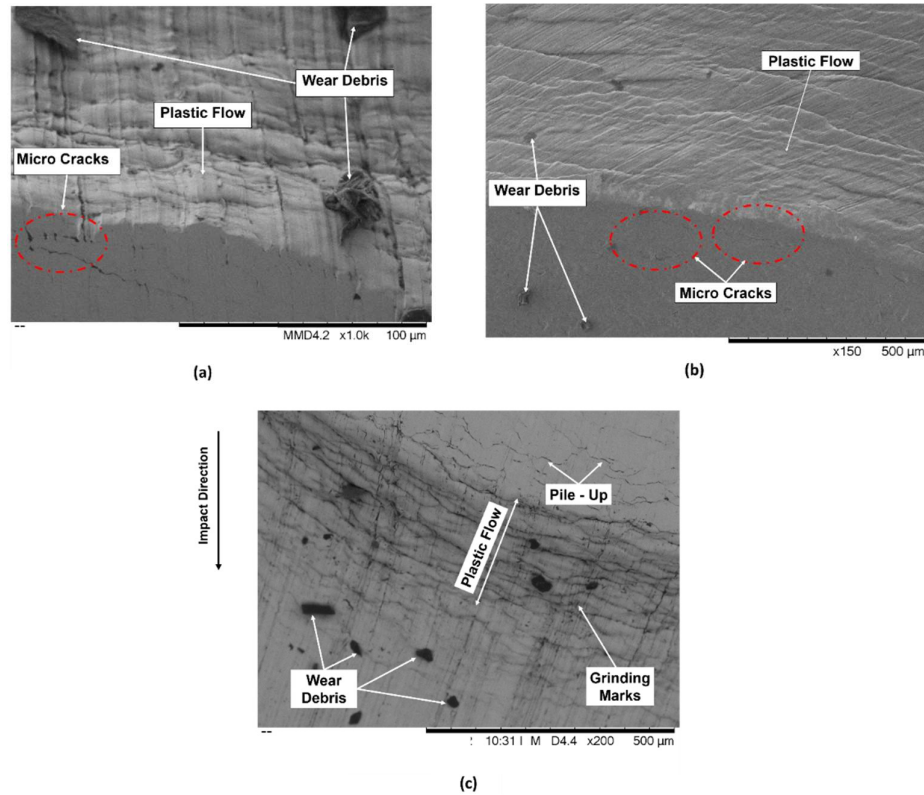


Figure 16 - Plastic flow formation on the edges and micro-cracks after 36,000 cycles for tested materials after 36000 cycles for (a) ductile cast iron, (b) aluminium alloy and (c) medium carbon steel.

4.5 Micro Hardness Measurements

Micro-hardness profiles of the subsurface material resulting from the impact wear process after 36,000 cycles were obtained by Struers Durascan Vickers indentation where loading and unloading were performed with a holding period of 10s and distance between indentations was 2.5d, according to ASTM E384 [18], at the maximum load of 0.1kgf for all materials.

Figure 17 shows microhardness measurements at a position below the maximum indentation depth of the impact scar and the error bar representing the standard deviation of the data from three repetitions for each distance from the surface.

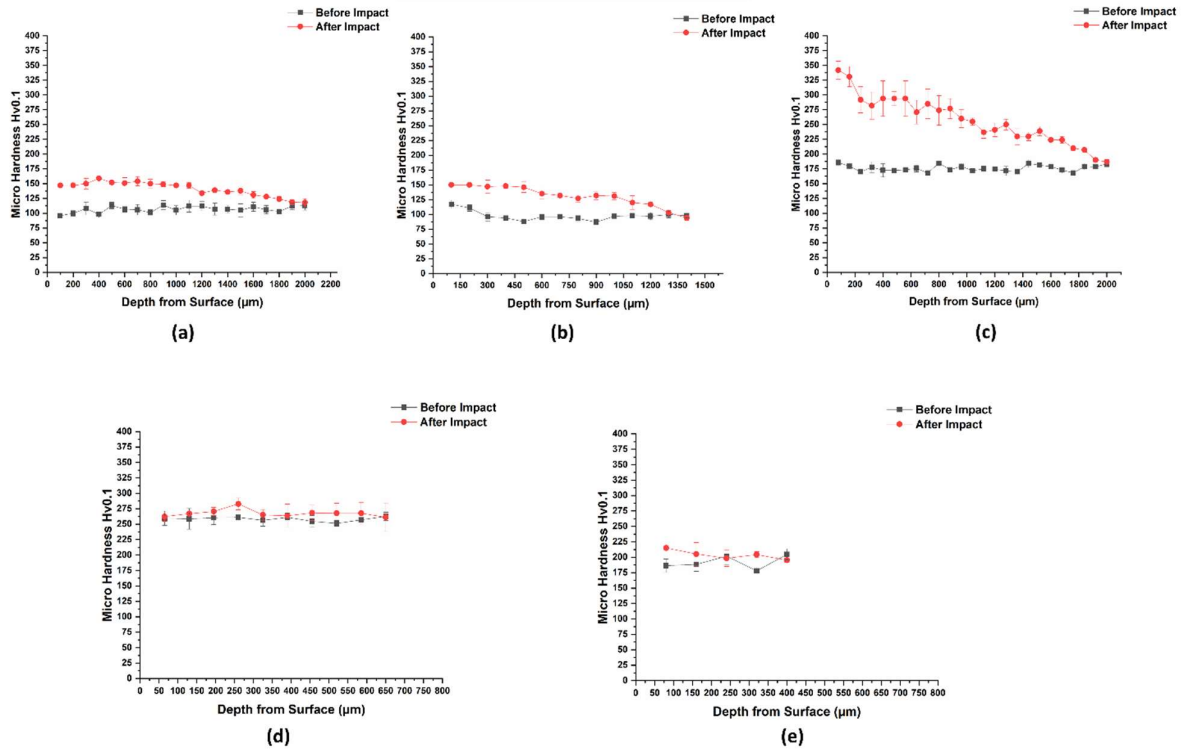


Figure 17 - Microhardness measurements for (a) aluminium alloy, (b) phosphor bronze, (c) austenitic stainless steel, (d) ductile cast iron and (e) medium carbon steel.

Based on the measurements, aluminium alloy, phosphor bronze and austenitic stainless steel showed a significant increase in hardness after 36,000 cycles of impact due to the role of work hardening resulting from the repetitive impact, while both medium carbon steel and ductile cast iron have more plastic flow on the scar ridges with significant increase in hardness of plastic flow and recording an average increase of 24% for ductile cast iron with a similar pattern for medium carbon steel, both materials did not show a significant increase in hardness for the centre of the wear scar as appeared in Figure 17.

The average observed increases in hardness for phosphor bronze, aluminium alloy and austenitic stainless steel were 36%, 31% and 34% respectively and reached depths of approximately 1.4mm-2mm from the surface as the microhardness results showed, which indicate strain hardening of the materials.

The current results revealed an increase in hardness which agrees with previous results of Rastegar [19] and Yilmaz [20].

An example of the grain deformation that typically occurs near the bottom edge of a medium carbon steel impact scar is shown in Figure 18, which shows the deformed grains of both ferrite (α) and pearlite (P). Also visible is a microhardness indentation which represents a value of 257Hv.

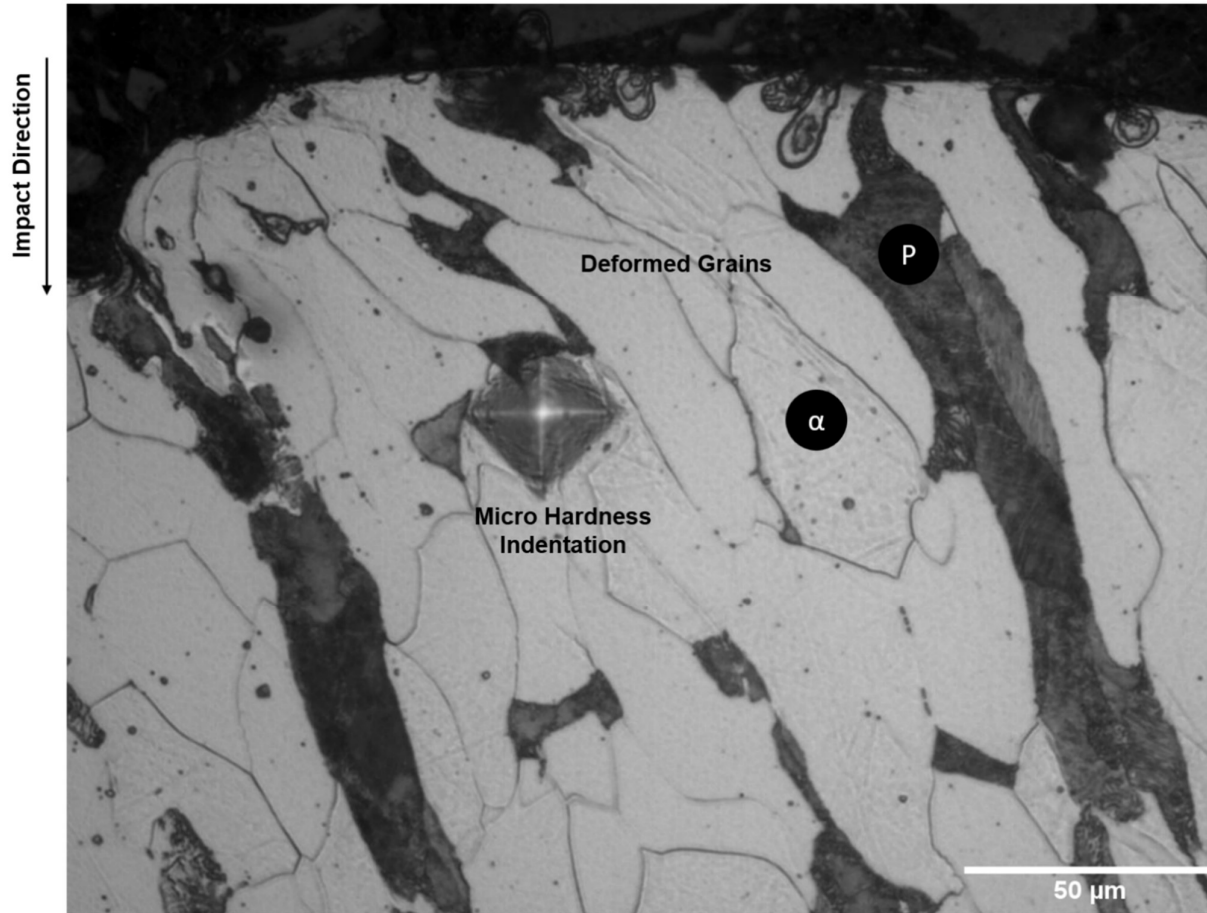


Figure 18 - Microhardness indentation of medium carbon steel below the bottom edge of wear scar after 36,000 cycles.

5. Discussion

These results for volume loss are in agreement with the work of Engel [5] in that there are a number of wear cycles that a surface can undergo before it starts to present as a worn surface in the traditional sense. It is proposed in this work that this is defined as a zero wear volume and that it can occur at any point instead of after a number of cycles from the initial contact. This is justified by these results demonstrating that this not only occurs in the elastic region, and that the materials can undergo further plastic deformation without any mass loss.

For the case of the stainless steel used in this work there was no mass loss found after up to 16,800 cycles, yet an apparent plastically deformed region formed on the surface of the specimen and large scar after further impacts were accumulated. Further evidence is that the wear volume after 36,000 cycles (mass scale) was very small compared with the total volume loss measured by profilometry, thus proving that there is a significant volume being compressed rather than removed from material.

The current results suggest that the previous results of papers that used the 3D non-contact profilometer to calculate the wear volume loss such as by Matti [21], Jiang[22] and Vahid[19], should also have used a mass scale in conjunction with Equation 6 in order to find the zero wear volume. This is especially the case when impact occurs normal to the surface and the materials under investigation are expected to be significantly compressed due to their ductility and therefore this volume cannot be neglected when measuring the total volume loss.

The work also suggests that ferrous and non-ferrous materials tested appear to be (locally) compressible and this contributes to the overall wear volume lost, a role not widely reported. This may be due to localised microstructural defects (void nucleation, dislocation, coalescence, internal porosity from ductile failure) and changes (phase transformation, carbide precipitation or hardening).

Surface and subsurface examination by SEM revealed that the main damage mechanism for tested materials was mainly plastic deformation and surface fatigue due to spalling as a result of the formation of small pits and then subsequent microcracks. There was no obvious delamination or material transfer to the impact striker observed in any of the materials. The small scale pitting which led to spalling is expected since the mass loss was very small for all materials and this contributed to the role of zero wear volume during impact.

The current results revealed that the zero wear volume is inversely proportional to the bulk hardness of material. Figure 10 shows that ductile cast iron, which has the highest hardness, has the least zero wear volume whereas the aluminum alloy, with lower hardness, has the greatest zero wear volume.

Hardness, however, appears not to be a primary parameter affecting the mass loss of materials under normal impact. Figure 8 shows that ductile cast iron has more mass loss than both medium carbon steel and austenitic stainless steel despite its relatively higher hardness. This agrees with the previous findings of Rabinowicz [15]. The results also showed no direct correlation between the Young's modulus or bulk hardness of the materials and wear volume for any materials which is accounted for by the zero wear.

The current results show that the austenitic stainless steel (AISI 304) has the greatest ability to work harden among other tested materials and the increase in hardness near the surface for the centre of the impact scar is almost twice the original bulk hardness. Similar results for the same materials were also observed by Fricke [23] where the surface microhardness results of austenitic stainless steel (also AISI 304) increased from 242Hv to approximately 650Hv which indicates the great capacity for work hardening. This could explain the greater propensity of austenitic stainless steel to appear to be compressed as zero wear volume. With similar consideration of the relative material properties of the other materials studied here, and their performance in these tests, it could be concluded that the material with the largest ability to work hardening is more likely to have more zero wear volume than other materials.

Results in Table 4 reveal possible correlation between material ductility and plastic flow formation for ferrous materials. Higher ductility leads to greater zero wear volume (i.e. more material is compressed for a given impact) and eventually reduced both plastic flow and wear volumes. Both medium carbon steel and ductile cast iron (both with low ductility) showed more plastic flow of material at the wear scar edges compared to austenitic stainless steel. Since the nature of impact is compression under normal impact therefore, microhardness examination revealed strain hardening as expected for all materials under repetitive impacts.

6. Conclusions

Conclusions arising from this work are as follows:

1. Neither Young's modulus nor bulk hardness has direct correlation with wear volume resulting from single repetitive normal impacts for the materials considered here.
2. Bulk hardness is inversely proportional to both zero wear volume and maximum indentation resulting from repetitive normal impacts for the materials considered here.
3. All materials show relatively very small amounts of wear volume loss compared with zero wear volume or plastic flow volume, in their total volume loss.

4. Mass scale and direct volume measurements by non-contact 3D profilometer should both be used in subsequent studies of this nature to detect the possible zero wear volume, as it would otherwise be neglected.

Acknowledgements

Mohanad Zalzalah would like to acknowledge the support of: Iraqi Ministry of Oil and LUKOIL.

References

- [1] P. A. Engel and F. F. Ling, "Impact Wear of Materials," ed: American Society of Mechanical Engineers Digital Collection, 1978.
- [2] P. A. Engel, "Impact Wear of Materials" vol. 2: Elsevier, 1978.
- [3] P. Engel, "Analysis and Design for Zero Impact Wear," Journal of Lubrication Technology JULY, p. 455, 1974.
- [4] P. Engel, "Percussive impact wear: A study of repetitively impacting solid components in engineering," Tribology International, vol. 11, pp. 169-176, 1978.
- [5] P. Engel, T. Lyons, and J. Sirico, "Impact wear model for steel specimens," Wear, vol. 23, pp. 185-201, 1973.
- [6] T. Slatter, H. Taylor, R. Lewis, and P. King, "The influence of laser hardening on wear in the valve and valve seat contact," Wear, vol. 267, pp. 797-806, 2009.
- [7] R. Lewis, C. Tsoraki, J. Broughton, J. Cripps, S. Afodun, T. Slatter, et al., "Abrasive and impact wear of stone used to manufacture axes in Neolithic Greece," Wear, vol. 271, pp. 2549-2560, 2011.
- [8] T. Bruce, H. Long, T. Slatter, and R. Dwyer-Joyce, "Formation of white etching cracks at manganese sulfide (MnS) inclusions in bearing steel due to hammering impact loading," Wind Energy, vol. 19, pp. 1903-1915, 2016.
- [9] T. Slatter, "Reducing Automotive Valve Recession with Surface Treatment," PhD Thesis, University of Sheffield, 2010.
- [10] K. L. Johnson and K. L. Johnson, "Contact Mechanics", Cambridge University Press, 1987.
- [11] J. E. Shigley, "Shigley's Mechanical Engineering Design", Tata McGraw-Hill Education, 2011.
- [12] W. J. Stronge, "Impact Mechanics", Cambridge University Press, 2018.
- [13] R. J. Dwyer-Joyce, "Tribological Design Data Part 3: Contact Mechanics," University of Sheffield 1997.
- [14] J. Williams, "Engineering Tribology", Cambridge University Press, 2005.
- [15] E. Rabinowicz, "Friction and Wear of Materials," 1995.
- [16] Z. Wang, Z.-b. Cai, Z.-q. Chen, Y. Sun, and M.-h. Zhu, "Low-velocity impact wear behavior of ball-to-flat contact under constant kinetic energy," Journal of Materials Engineering and Performance, vol. 26, pp. 5669-5679, 2017.
- [17] T. Slatter, R. Lewis, and A. H. Jones, "The influence of cryogenic processing on wear on the impact wear resistance of low carbon steel and lamellar graphite cast iron," Wear, vol. 271, pp. 1481-1489, 2011.
- [18] D. W. Hetzner, "Microindentation hardness testing of materials using ASTM e384," Microscopy and Microanalysis, vol. 9, pp. 708-709, 2003.
- [19] V. Rastegar and A. Karimi, "Surface and subsurface deformation of wear-resistant steels exposed to impact wear," Journal of materials engineering and performance, vol. 23, pp. 927-936, 2014.
- [20] H. Yilmaz and R. Sadeler, "Impact wear behavior of ball burnished 316L stainless steel," Surface and Coatings Technology, vol. 363, pp. 369-378, 2019.
- [21] M. Lindroos, V. Ratia, M. Apostol, K. Valtonen, A. Laukkanen, W. Molnar, et al., "The effect of impact conditions on the wear and deformation behavior of wear resistant steels," Wear, vol. 328, pp. 197-205, 2015.

- [22] W. Jiang, C. Liu, C. He, J. Guo, W. Wang, and Q. Liu, "Investigation on impact wear and damage mechanism of railway rail weld joint and rail materials," *Wear*, vol. 376, pp. 1938-1946, 2017.
- [23] R. Fricke and C. Allen, "Repetitive impact wear of steels," *Wear*, vol. 162, pp. 837-847, 1993.